

Article

Estimating Daily Temperatures over Andhra Pradesh, India, Using Artificial Neural Networks

Gubbala Ch. Satyanarayana ¹, Velivelli Sambasivarao ¹, Peddi Yasaswini ¹  and Meer M. Ali ^{1,2,3,*} 

¹ Center for Atmospheric Science, Electronics and Communication Engineering, Koneru Lakshmaiah Education Foundation, Guntur 522501, India; gcsatya@kluniversity.in (G.C.S.); sambasivavelivelli@gmail.com (V.S.); peddiyasaswini@gmail.com (P.Y.)

² Andhra Pradesh State Disaster Management Authority (APSDMA), Guntur 522501, India

³ Center for Ocean-Atmospheric Prediction Studies (COAPS), Florida State University, Tallahassee, FL 32306-2741, USA

* Correspondence: mmali@coaps.fsu.edu

Abstract: In the recent past, Andhra Pradesh (AP) has experienced increasing trends in surface air mean temperature (SAT at a height of 2 m) because of climate change. In this paper, we attempt to estimate the SAT using the GFDL-ESM2G (Geophysical Fluid Dynamics Laboratory Earth System Model version 2G), available from the Coupled Model Intercomparison Project Phase-5 (CMIP5). This model has a mismatch with the India Meteorological Department (IMD)'s observations during April and May, which are the most heat-prone months in the state. Hence, in addition to the SAT from the model, the present paper considers other parameters, such as mean sea level pressure, surface winds, surface relative humidity, and surface solar radiation downwards, that have influenced the SAT. Since all five meteorological parameters from the GFDL-ESM2G model influence the IMD's SAT, an artificial neural network (ANN) technique has been used to predict the SAT using the above five meteorological parameters as predictors (input) and the IMD's SAT as the predictand (output). The model was developed using 1981–2020 data with different time lags, and results were tested for 2021 and 2022 in addition to the random testing conducted for 1981–2020. The statistical parameters between the IMD observations and the ANN estimations using GFDL-ESM2G predictions as input confirm that the SAT can be estimated accurately as described in the analysis section. The analysis conducted for different regions of AP reveals that the diurnal variations of SAT in the IMD observations and the ANN predictions over three regions (North, Central, and South AP) and overall AP compare well, with root mean square error varying between 0.97 °C and 1.33 °C. Thus, the SAT predictions provided in the GFDL-ESM2G model simulations could be improved statistically by using the ANN technique over the AP region.

Keywords: ANN model; CMIP5; GFDL-ESM2G; surface air mean temperature; summer season



Citation: Satyanarayana, G.C.; Sambasivarao, V.; Yasaswini, P.; Ali, M.M. Estimating Daily Temperatures over Andhra Pradesh, India, Using Artificial Neural Networks. *Atmosphere* **2023**, *14*, 1501. <https://doi.org/10.3390/atmos14101501>

Academic Editor: Jaroslaw Krzywanski

Received: 12 August 2023

Revised: 16 September 2023

Accepted: 25 September 2023

Published: 28 September 2023



Copyright: © 2023 by the authors. Licensee MDPI, Basel, Switzerland. This article is an open access article distributed under the terms and conditions of the Creative Commons Attribution (CC BY) license (<https://creativecommons.org/licenses/by/4.0/>).

1. Introduction

Andhra Pradesh (AP) has been experiencing heating trends in the recent past and is one of the states that are most vulnerable to increasing temperatures in India. This is primarily because of climate change, with temperatures increasing quasi-linearly with cumulative greenhouse gas emissions [1–3]. Coupled-model future projections indicate that the mid-century temperature would rise and exceed the average temperature compared to the baseline period (1976–2005) by about 1.9 °C in the Indian subcontinent [3]. Earlier studies suggest that, in India, annual and seasonal surface air mean temperatures at a 2m height (hereafter referred to as SAT) are projected to increase with global warming [3]. In recent decades, many researchers have focused on long-term SAT changes/trends in India because of global warming [4–6]. Here, we studied the rise in temperature over the AP region alone.

It may be preferable to investigate and use other modeling approaches, such as data-driven models, rather than creating a conceptual model. In the data-driven method, models built on differential equations are used to find the best input–output mapping without fully analyzing the underlying structure of the phenomenon. Data-driven models have been proven to provide reliable forecasts in a variety of fields [7–9].

Artificial intelligence and machine learning methods have recently been used to forecast the weather at various time scales [10–17]. The review papers by Cifuentes et al. [18] and Fan et al. [19], as well as the references included therein, demonstrate the expanding use of machine learning approaches to comprehend and forecast the climate at various time scales.

One of the most crucial elements of soft computing is the artificial neural network (ANN). They are employed for data processing, analysis, and replication of brain activity. The ANNs' capacity for self-learning enables them to compute precise solutions to issues that are challenging to answer using conventional analytical techniques. They can respond to complex nonlinear models without imposing any constraints or presumptions on the incoming data, which they can comprehend and learn without the need for reprogramming. They can also understand missing data, be readily maintained, have excellent accuracy, and be implemented on parallel hardware. Neural network-based algorithms and stochastic approaches have attracted a lot of attention recently in the domains of computer science, and engineering due to their robustness and efficacy. The ANN has been widely utilized in several study fields and has aided in the solution of challenging issues. Scientists have recently been interested in ANN modeling because it produces excellent results for forecasting factors linked to temperatures [20–22].

A common approach among the previous studies predicting meteorological parameters is to apply global climate models from different assessment reports, made by the Intergovernmental Panel on Climate Change (IPCC), to evaluate temperature changes. Under the framework of the coupled model inter-comparison project (CMIP), many climate simulations have been performed and released widely. Previous experiments (i.e., CMIP3) have been utilized in several studies [23–26]. The results of recent regional evaluations have demonstrated that the CMIP Phase-5 (CMIP5) outputs have improved compared to the previous phases [27].

The GFDL-ESM2G (Geophysical Fluid Dynamics Laboratory Earth System Model version 2G), one of the models from the CMIP5, consists of a single output with a single simulation (i.e., from a single ensemble (r1i1p1) member of a single climate experiment). Mohan and Bhaskaran [28] reported that this is one of the three best models among all the CMIP5 models. Here, we used this model to improve the SAT predictions through a neural network technique by using other meteorological factors that influence the SAT. This model has been used for the Indian region in several studies [28–31]. However, this single output has a mismatch with the India Meteorological Department (IMD)'s observations, as discussed in the results section.

Astsatryan et al. [32] used an ANN approach to forecast air temperature 3 to 24 h in advance. They used hourly air pressure, relative humidity, wind speed, and dew point temperature as inputs to the model. Their accuracies varied from 3.37 °C to 3.55 °C in terms of the root mean square error (RMSE). The present study considers mean sea level pressure, surface winds, surface relative humidity, and surface solar radiation downwards to predict the SAT available from the GFDL-ESM2G 10 days in advance through an ANN technique. In this technique, IMD observations are used as the predictand (output) during April and May, which are the state's most heat-prone months. The following sections examine the study's data and methods before presenting the results.

2. Data and Methodology

2.1. Data

All the meteorological parameters (10 m level wind, 2 m temperature—SAT, mean sea level pressure, surface relative humidity, and surface solar radiation downwards—insolation)

gridded data are obtained globally from the CMIP5 GFDL-ESM2G model simulations [33]. These data are the daily global atmospheric parameters from 1981 to 2022 at a 0.25-degree resolution in a NetCDF format, which are derived from the historical and future runs of CMIP5 model simulations. The IMD's gridded daily mean temperature data at a 1.0-degree resolution [34] for the same period are also used in this study. While the CMIP5 data are at a 0.25-degree resolution, the IMD observations are available at a 1.0-degree resolution. Hence, the CMIP5 data have been re-gridded to a 1.0-degree resolution using a Climate Data Operator (CDO), as shown in Figure 1.

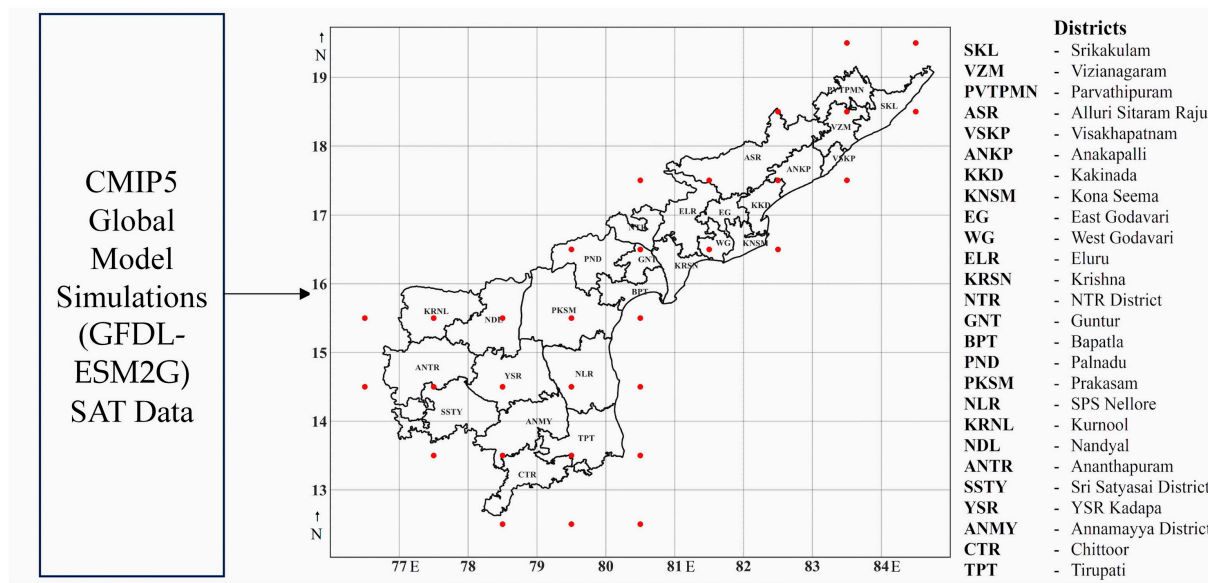


Figure 1. Study area and number of grids used in the present study. The red dots indicate the center of the grid. The grid points outside the boundary are used for interpolation.

2.2. Methodology

The re-gridded GFDL-ESM2G model's and IMD observations' data at a 1-degree spatial resolution that were in NetCDF form were converted to comma-separated values. We had 30 grid points in the study area, as shown in Figure 1. It was observed that the model data had random errors. To remove these random errors in the input data, we applied a ± 3 -sigma (or \pm three times the standard deviation of a parameter) filter to the input data and rejected all the records in which any of the six parameters had more/less than 3-sigma values. We did not apply this elimination criteria to the dependent temperature from the IMD, as this parameter would not have been available during the prediction period. The total number of data points available from 1981 to 2022 was 65,591. After this filtering, these points were reduced to 46.5% (35,076) of the original data. This means that the model simulations had a significant number of random errors.

2.2.1. ANN Approach

Before selecting the ANN approach, we estimated SAT using the random forest and multiple regression methods. The RMSE values for the above two approaches were 1.33 and 1.45, and the multiple correlation coefficient (R) values were 0.68 and 0.64, respectively, while these values with the ANN approach were 1.22 and 0.8. Hence, we selected the ANN approach for our analysis. The ANN is an information-processing computer model consisting of simple processing units called artificial neurons. The ANN consists of interconnected nodes whose functionality is based on neurons [35]. This technique was used in studies related to meteorological [36–38], oceanographic [35,39,40], and satellite parameter retrievals [41–43]. The ANN technique is superior to the multiple regression approach [35]. The ANN analysis requires three sets of data: (1) training; (2) testing; and

(3) validation. The training dataset is used to train the model and the testing dataset is used to test the model. Any shortcomings during the training process are adjusted during the testing stage so that the model does not overfit during training. The model verifies, at this stage, whether the model developed from the training dataset holds well outside the training data range, in terms of RMSE, and applies a midterm correction if required. Finally, the model developed during training and testing is stored and used for validation. The validation data is independent and not used during training or testing. The radial basis functions (RBF) and the multi-layer perceptron (MLP) are the two popular ANN models in which both the input and the output variables are normalized to vary between zero and one. The present ANN architecture has one input layer with six neurons, one hidden layer with twenty-five neurons, and one output layer with one neuron. The six neurons in the input layer consist of five model simulations and one climatological mean value (Figure 2).

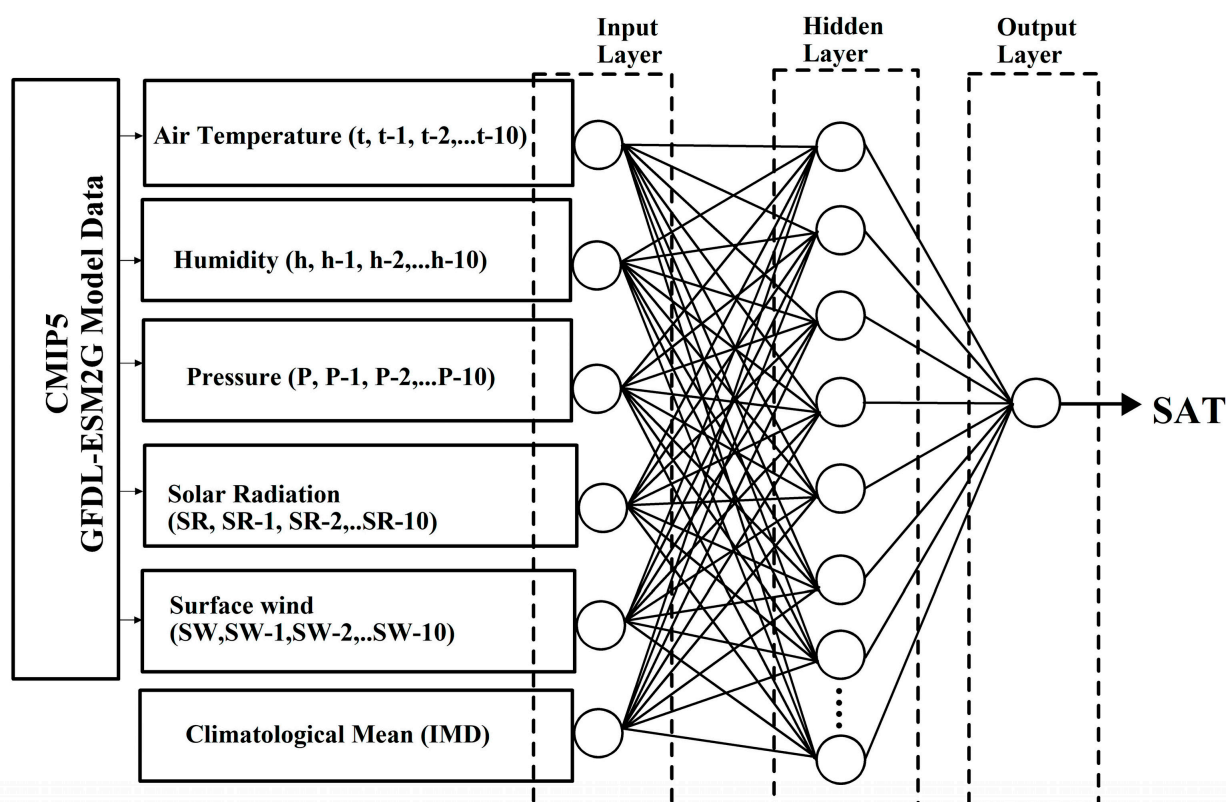


Figure 2. ANN model architecture with six neurons in the input layer, twenty-five neurons in the hidden layer, and one neuron in the output layer.

The climatological parameter is considered to be one of the inputs because a variable fluctuates around its climatological value. We attempted both the MLP and RBF models and found that the MLP provided better results compared to the RBF in terms of RMSE. Similarly, the exponential function for the hidden neurons and the identity function for the output neurons yielded better results in terms of RMSE compared to the other functions. Hence, we selected the MLP model with the exponential and identity functions. To overcome the overfitting and under-fitting problems, weight decay functions were used for the hidden and output layers. In addition, we also compared the statistical results of the training, testing, and validation datasets, which were almost similar. Hence, this ANN model did not encounter overfitting or underfitting problems.

2.2.2. Analysis

Since the ANN needs three sets of data, we randomly selected 70% of the data for training, 15% for testing, and 15% for validation following [44]. The random selection

avoided any bias that might have crept into the training of the ANN model had the training dataset been selected based on any other specific criteria. The independent variables or inputs (predictors) to the ANN model were as follows: (i) SAT; (ii) surface relative humidity; (iii) surface solar radiation downwards (insolation); (iv) surface wind at a height of 10 m; (v) mean sea level pressure; and (vi) climatological mean SAT. These parameters were selected because only these six parameters influence the SAT. All these input parameters were obtained from the CMIP5 during 1981–2022. The climatological mean value for the day was also considered as one of the inputs because the ambient temperature generally fluctuates around the climatological mean. The dependent variable or output (predictand) was the IMD's SAT during the same period.

To check how much these model-predicted meteorological parameters (SAT, surface wind, relative humidity, mean sea level pressure, and solar radiation) influenced the IMD-observed temperature, a statistical analysis was carried out. The R and RMSE between IMD observations as the predictand and all the above five model-derived parameters and the climatological SAT as the predictors were computed. Then, one parameter, say SAT, was removed and, again, R was obtained with the six predictors. In the next step, another parameter was removed by keeping back the SAT. This analysis was repeated for all six variables. Ray et al. [43] carried out a similar analysis for variance. In our study, we followed the similar approach. These parameters, apart from the SAT, have an impact on the observed SAT, as shown by an increase in the RMSE and a fall in the R when one predictor is eliminated at a time.

Data from 1981 to 2020 were used for training, testing, and validation when developing the ANN model, as mentioned earlier. The validation data was independent of training and testing. The result of this analysis is discussed in the results section. We wanted to test how many past model simulations were required to predict the observed SAT. For this purpose, past observations of different periods were selected. For example, the previous 1-day to the previous 10-day input parameters from the model are trained with the present-day IMD observations. Thus, the IMD observation over a location on the 11th May is trained with all the following input parameters: 1–10 May (Test-1), 2–10 May (Test-2), 3–10 May (Test-3), 4–10 May (Test-4), and 5–10 May (Test-5). The purpose of this type of analysis is to test which lead time period has a better prediction.

The statistical metrics of bias, RMSE, mean absolute percentage error (MAPE), index of agreement (IOA), correlation coefficient (CC), and scatter index (SI) were computed to evaluate the model's performance in the prediction of temperatures during the period of this study (Tables 1–3). The equations/formulae [44] used to compute these statistical parameters were as follows:

$$\text{BIAS} = \frac{1}{n} \sum (\text{Actual} - \text{Forecast}) \quad (1)$$

$$\text{CC} = \frac{\sum_{i=1}^n (f_i - \bar{f})(o_i - \bar{o})}{\sqrt{\sum_{i=1}^n (f_i - \bar{f})^2} \sqrt{\sum_{i=1}^n (o_i - \bar{o})^2}} \quad (2)$$

$$\text{MAPE} = \frac{1}{n} \sum_{i=1}^n \frac{|o_i - f_i|}{o_i} \times 100 \quad (3)$$

$$\text{RMSE} = \sqrt{\frac{\sum_{i=1}^n (f_i - o_i)^2}{n}} \quad (4)$$

$$\text{IOA} = 1.0 - \frac{\sum_{i=1}^n (f_i - o_i)^2}{\sum_{i=1}^n (|f_i - \bar{o}| + |o_i - \bar{o}|)^2} \quad (5)$$

$$\text{SI}(\%) = \frac{\text{RMSE}}{\frac{1}{n} \sum_{i=1}^n o_i} \times 100 \quad (6)$$

where o_i , f_i , and \bar{o} correspond to observations, forecast values, and observation mean.

Table 1. Statistical metrics of mean absolute percentage error (MAPE), root mean square error (RMSE), correlation coefficient (CC), bias, index of agreement (IOA), and scatter index (SI) between the ANN model predictions and the GFDL-ESM2G model output with observations (IMD) for the entire study region.

	MAPE	RMSE	CC	BIAS	IOA	SI (%)	Observed Mean	Predicted Mean
GFDL-ESM-2G	6.21	2.46	0.18	−0.53	0.49	7.75	31.72	31.18
ANN	2.75	1.12	0.79	0	0.87	3.53	31.72	31.73

Table 2. Statistical metrics of mean absolute percentage error (MAPE), root mean square error (RMSE), correlation coefficient (CC), bias, index of agreement (IOA), and scatter index (SI) for the ANN model with different lead time forecasts from 1981 to 2020 (April and May).

	MAPE	RMSE	CC	BIAS	IOA	SI (%)	Observed Mean	Predicted Mean
Test-1 (1–10 day period)								
Training	2.68	1.09	0.8	0	0.88	3.43	31.72	31.72
Testing	2.89	1.18	0.77	0.02	0.86	3.71	31.73	31.74
Validation	2.93	1.22	0.74	0	0.85	3.84	31.73	31.73
Test-2 (2–10 day period)								
Training	2.77	1.12	0.79	0	0.87	3.53	31.72	31.72
Testing	2.95	1.19	0.77	0.02	0.86	3.75	31.73	31.74
Validation	2.99	1.23	0.74	0.02	0.84	3.87	31.73	31.71
Test-3 (3–10 day period)								
Training	2.87	1.16	0.77	0	0.86	3.65	31.72	31.72
Testing	2.97	1.21	0.75	0.01	0.85	3.81	31.73	31.73
Validation	3.01	1.23	0.74	−0.02	0.84	3.87	31.73	31.72
Test-4 (4–10 day period)								
Training	2.86	1.16	0.77	0	0.86	3.65	31.72	31.72
Testing	2.95	1.21	0.76	−0.01	0.85	3.81	31.73	31.72
Validation	3.01	1.25	0.73	−0.01	0.84	3.93	31.73	31.72
Test-5 (5–10 day period)								
Training	2.94	1.19	0.75	0	0.84	3.75	31.72	31.72
Testing	3.04	1.23	0.74	0	0.84	3.87	31.73	31.73
Validation	3.04	1.26	0.72	0	0.83	3.97	31.73	31.73

Table 3. Statistical metrics of mean absolute percentage error (MAPE), root mean square error (RMSE), correlation coefficient (CC), bias, index of agreement (IOA), and scatter index (SI) for different ranges of temperature in model validation dataset.

Different Ranges in °C	MAPE	RMSE	CC	BIAS	IOA	SI (%)	Observed Mean	Predicted Mean
34–36 °C	3.41	1.35	0.37	−0.97	0.42	3.89	34.68	33.71
32–34 °C	2.63	1.09	0.36	−0.43	0.51	3.32	32.83	32.40
30–32 °C	2.34	0.98	0.32	0.16	0.54	3.15	31.09	31.25
28–30 °C	3.76	1.42	0.27	0.95	0.41	4.85	29.24	30.19

3. Results

A comparison of the GFDL-ESM2G model predictions, the IMD observations, and the ANN predictions is shown in Figure 3. It is clear from the figure that the mismatch between the GFDL-ESM2G model output and the IMD observations is greater when compared with the ANN predictions. The statistical results of this comparison are given in Table 1. All the statistical parameters, when compared with the observations, are better in the ANN estimation, compared to the GFDL-ESM2G predictions (Table 1).

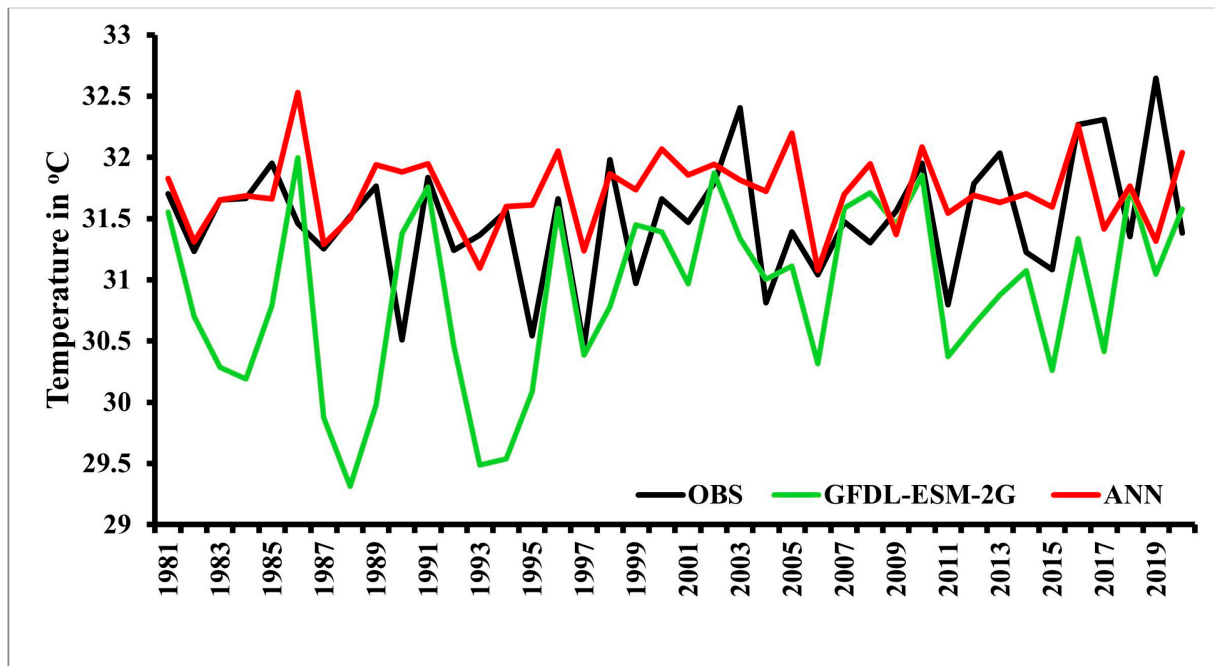


Figure 3. Time series of mean SAT (April–May) over the AP region for IMD observations (OBS), GFDL-ESM2G model output, and ANN model predictions for the period from 1981 to 2020.

From here on, only the validation dataset is discussed. The statistical results (Table 2) are almost similar for different periods of input. However, the errors increase with increased lead time. For example, the RMSE slightly increased by 0.04 °C from 1.22 °C for the 1–10 day period to 1.26 °C for the 5–10 day period in the validation dataset. The CC decreased from 0.74 for the 1–10 day duration to 0.72 for the 5–10 day input period in the validation dataset.

Similarly, the difference is very negligible for the other parameters as well. Considering the lower RMSE, higher CC, lower bias, and high IOA, we concluded that, the present ANN approach could be used to predict the temperatures at least 4 days in advance, which is a sufficient time-period to consider temperature-related hazards.

Variations of temperature during 1981–2020 for April and May for the five lead times along with the IMD observations are given in Figure 4a,b. The mean temperatures fluctuate from 31.1 °C to 32.2 °C in April and from 31.3 °C to 32.4 °C in May, indicating that the temperatures are slightly higher in May compared to April in all the years included in the study period. The fluctuations vary from year to year for all forecast durations from 1–10 days to 5–10 days in both months. The deviations between the predicted values and the observations are negligible, a fact which is also represented in the lower RMSE of the estimation (Table 2).

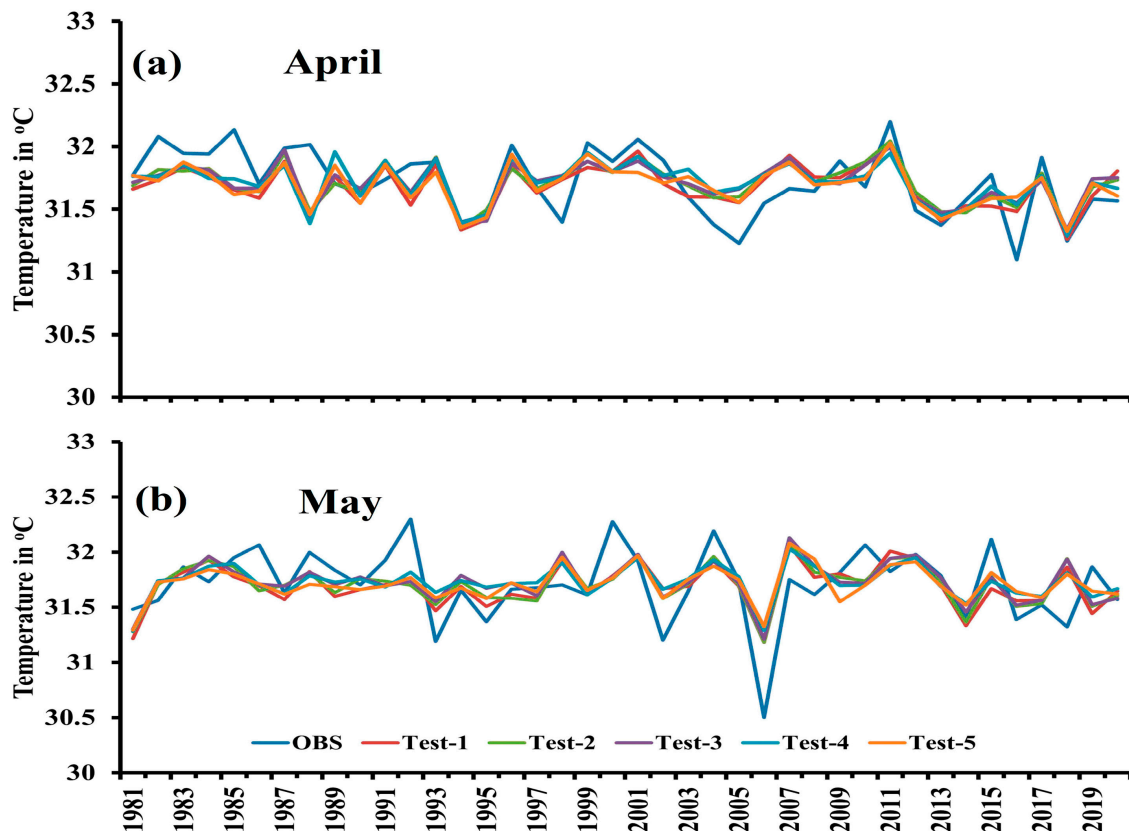


Figure 4. Variation of mean temperature predicted for the five lead time forecasts (Test-1, Test-2, Test-3, Test-4, and Test-5) along with IMD observations during 1981–2020 for (a) April and (b) May.

The spatial distribution of the average temperature during 1981–2020 of the validation datasets according to the ANN predictions and the IMD observations, as well as their difference, is given in Figure 5. On the one hand, when the temperatures are high both in the observations and the predictions, for example over Nellore, the difference between the two observations is negligible. On the other hand, when the temperatures are low in the estimations and observations, the difference is large. For further analysis, the temperatures were grouped into different categories; the statistical analysis was carried out for the validation dataset and is presented in Table 3. The MAPE, RMSE, SI, and Bias are relatively low for the 30–32 °C range compared to the other ranges.

In addition to the random validation conducted for the 1981–2020 time-period, the developed ANN model was also used to validate for the entire years of 2021 and 2022, and compare it with the IMD observations for three regions, South AP, Central AP, and North AP, as well as the entire AP (Figure 6). The RMSE, MAPE, and CC between the ANN and IMD observations are provided in the top right corner of each panel in Figure 6.

The daily fluctuations during April–May 2021 and 2022 in the three regions and for the state as a whole are presented in Figure 7. Most of the differences between the estimations and the observations (Figure 7) vary between -1.5 °C and 1.5 °C.

Most of the deviations are negative, indicating that the estimations are slightly lower than the observations. The diurnal variations of mean temperatures in the IMD observations and the ANN predictions over the three regions (North, Central, and South AP) and the overall AP compare well, with the RMSE varying between 0.94 °C and 1.33 °C.

The spatial distribution of the difference between the ANN predictions and the IMD observations for April and May in 2021 and 2022 is shown in Figure 8. Spatially, the difference varies between -3 °C and 2 °C. In April 2021, Central AP and, in April 2022, North AP were over-estimated in the ANN predictions while the predictions for the rest of AP were under-estimated compared to the observations.

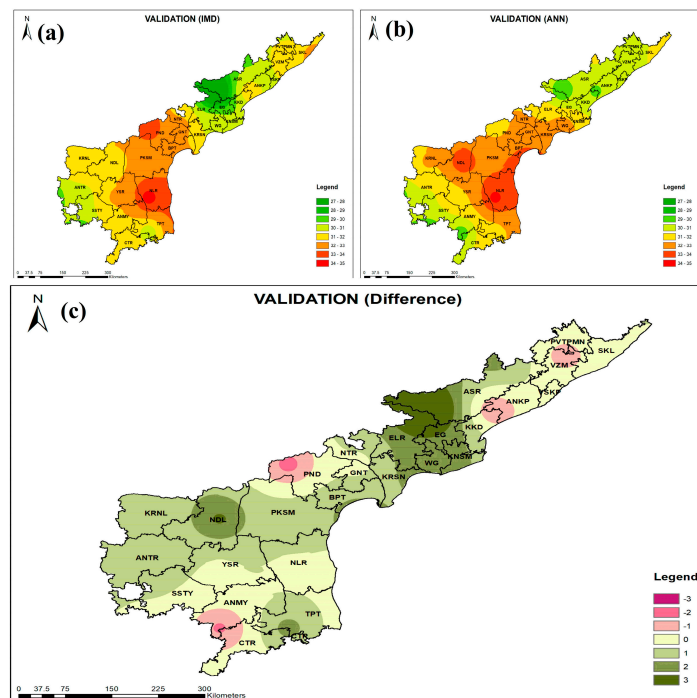


Figure 5. Spatial temperature distribution of validation dataset for (a) IMD observations, (b) ANN predictions, and (c) bias between the two values from 1981 to 2020 over AP (30 grids).

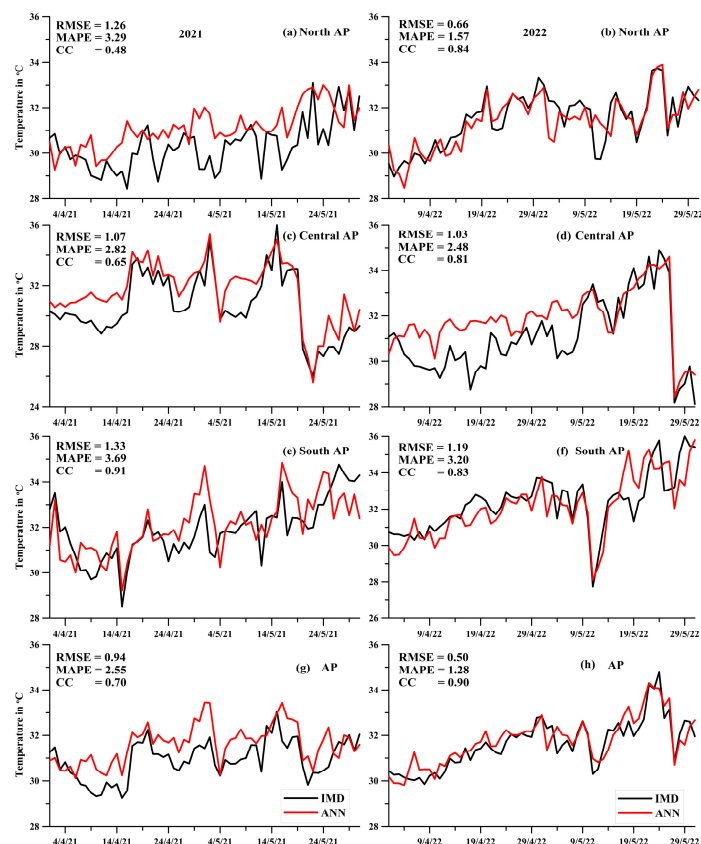


Figure 6. The temperature predicted using the ANN and IMD observations in different regions for 2021 and 2022: over North AP (a,b) with nine grids, Central AP (c,d) with nine grids, South AP (e,f) with twelve grids, and overall AP (g,h) with thirty grids. The RMSE, MAPE, and CC between the ANN and IMD observations are provided in the top right corner of each panel.

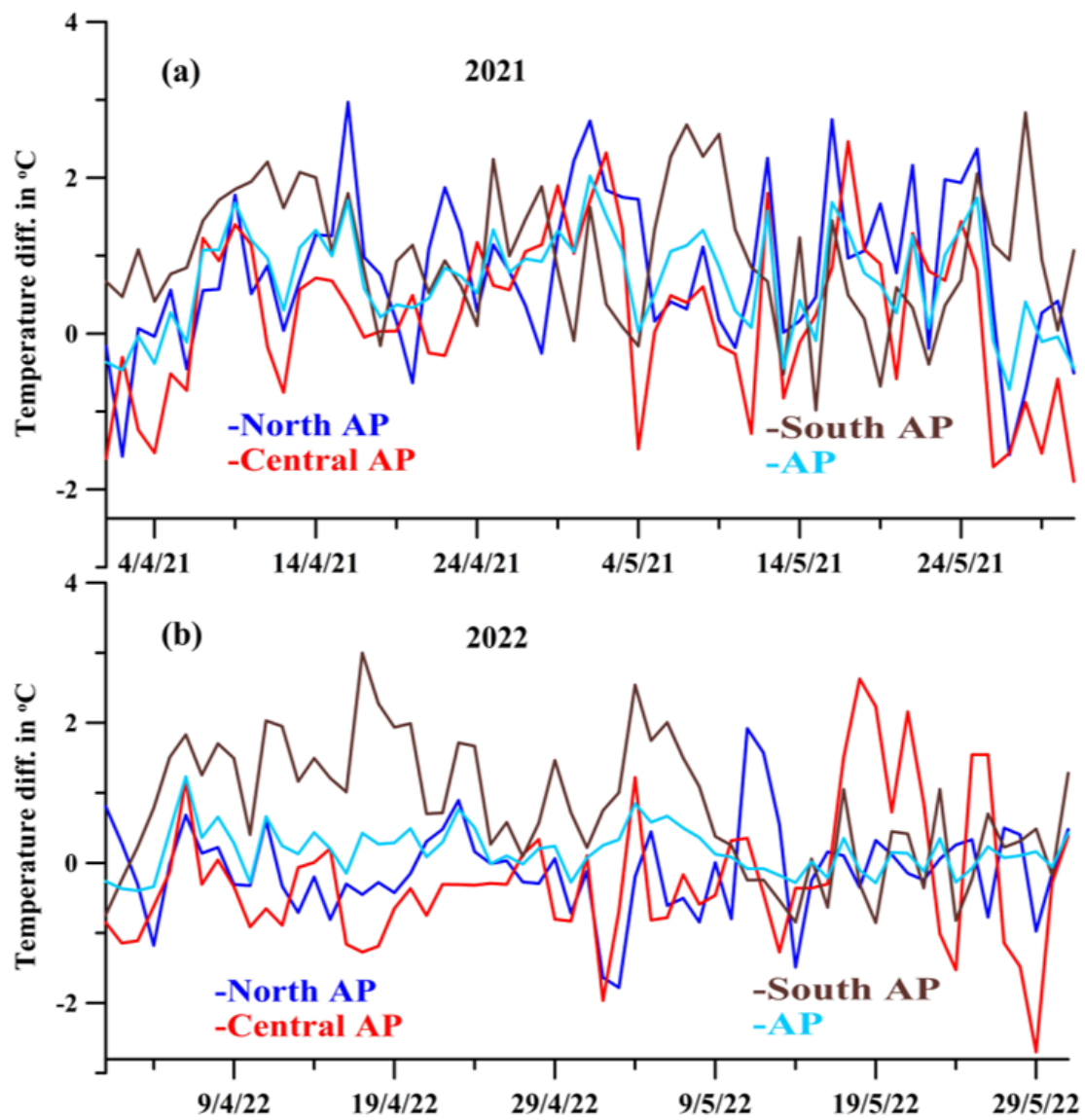


Figure 7. Difference between the ANN model and the IMD observations in different regions over AP for (a) 2021 and (b) 2022. The grid points in each region and the statistical metrics are provided in Figure 6.

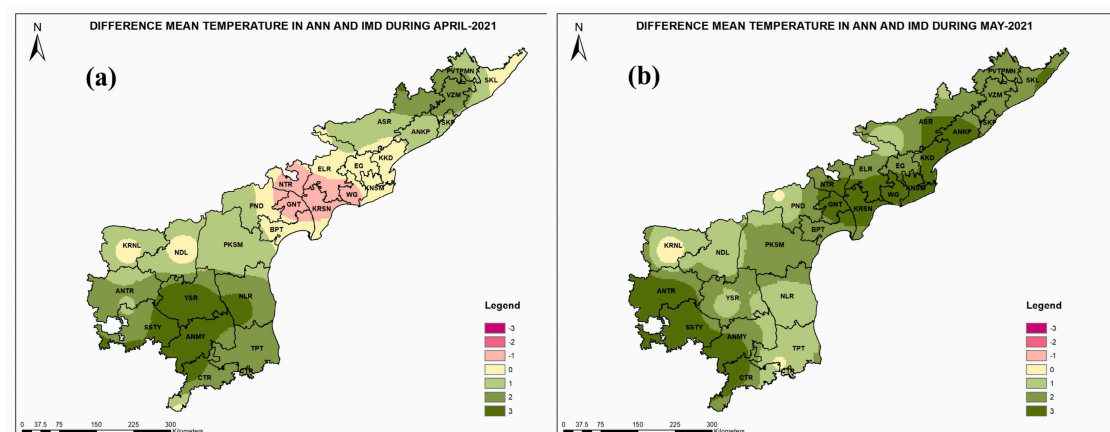


Figure 8. Cont.

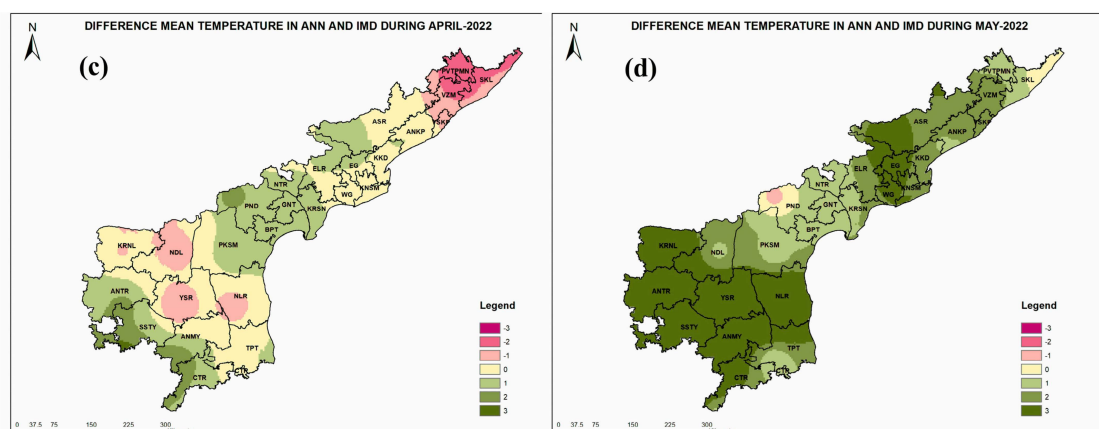


Figure 8. Spatial distribution of model bias (ANN model—observation) in (a) April 2021, (b) May 2021, (c) April 2022, and (d) May 2022.

4. Conclusions

The ANN approach was used to estimate the mean temperatures, SAT, over the AP region using the CMIP5 projections of mean surface temperatures, relative humidity, incoming solar radiation, surface winds, mean sea level pressure and climatological SAT as the predictors and the IMD observations as the predictand during April and May. The previous 1–10 day to the previous 5–10 day input parameters from the model were trained with the present-day IMD observations as described in the methodology section. The results reveal that CMIP5 projections can be conveniently used to predict temperatures with an accuracy of 1.2 °C RMSE, MAPE of 2.9 °C, CC of 0.7, and IOA of 0.8 for the validation dataset during the 1981–2020 time-period using the ANN technique.

The temperatures and fluctuations were slightly higher in May compared to April throughout the study period. A comparison of the 1981–2020 average observations over the AP region shows that the difference between the IMD observations and the ANN estimations is negligible when the temperatures are higher in the observations, whereas the difference is relatively large for lower temperatures. However, this difference varies between -2 °C and 2 °C over most of the places in AP. The diurnal variations of mean temperatures in the IMD observations and the ANN predictions over the three regions (North, Central, and South AP) and the overall AP compared well with the RMSE varying between 0.94 °C and 1.33 °C.

In addition to the random validation conducted for the 1981–2020 time-period, the validation carried out for the entire years of 2021 and 2022 and the comparison with the IMD observations revealed that the predictions for 2021 and 2022 varied between -1.5 °C and 1.5 °C. The spatial distribution of the model bias had a variation of -2 to $+2$ °C. Thus, the ANN model can be conveniently used to predict temperatures over the AP region using the CMIP5 projections of the meteorological parameters.

Author Contributions: Data downloading, curation, and analysis: V.S. and P.Y.; problem envision, methodology adoption, computation, software, visualization, data analysis, writing—review and editing: M.M.A. and G.C.S. All authors have read and agreed to the published version of the manuscript.

Funding: APSDMA, Government of AP under grant No. 10-12038/32/2021-ADMIN SEC-SDMA-REVD.M.

Institutional Review Board Statement: Not applicable.

Informed Consent Statement: Not applicable.

Data Availability Statement: All the data are available in the public domain.

Acknowledgments: Part of this research is funded by APSDMA, Government of AP under grant no. 10-12038/32/2021-ADMIN SEC-SDMA-REVD.M. The authors acknowledge the data from the India

Meteorological Department (IMD) and CMIP5 dataset, prepared by the Copernicus Climate Change Service (C3S). The authors acknowledge the support and encouragement given by the Andhra Pradesh State Disaster Management Authority (APSDMA), Government of AP, and the Koneru Lakshmaiah Education Foundation.

Conflicts of Interest: The authors declare that there are no conflict of interest.

References

1. Bhadram, C.V.; Amatya, B.V.; Pant, G.B.; Kumar, K.K. Heat waves over Andhra Pradesh: A case study of summer 2003. *Mausam* **2005**, *56*, 385–394. [[CrossRef](#)]
2. *Climate Change 2021—The Physical Science Basis*; Climate Change and Law Collection; Cambridge University Press: Cambridge, UK; New York, NY, USA, 2021.
3. Krishnan, R.; Sanjay, J.; Gnanaseelan, C.; Mujumdar, M.; Kulkarni, A.; Chakraborty, S. Correction to: Assessment of Climate Change over the Indian Region. In *Assessment of Climate Change over the Indian Region*; Springer: Singapore, 2021.
4. Solomon, S. *Climate Change 2007: The Physical Science Basis*; Cambridge University Press: Cambridge, UK, 2008.
5. Trenberth, K.E.; Jones, P.D.; Ambenje, P.; Bojariu, R.; Easterling, D.; Klein Tank, A.; Parker, D.; Rahimzadeh, F.; Renwick, J.A.; Rusticucci, M.; et al. Observations: Surface and Atmospheric Climate Change. In *Climate Change 2007: The Physical Science Basis. Contribution of Working Group I to the Fourth Assessment Report of the Intergovernmental Panel on Climate Change*; Solomon, S., Qin, D., Manning, M., Chen, Z., Marquis, M., Averyt, K.B., Tignor, M., Miller, H.L., Eds.; Cambridge University Press: Cambridge, UK; New York, NY, USA, 2007.
6. Vieira, F.F.; Oliveira, M.; Sanfins, M.A.; Garção, E.; Dasari, H.; Dodla, V.; Satyanarayana, G.C.; Costa, J.; Borges, J.G. Statistical analysis of extreme temperatures in India in the period 1951–2020. *Theor. Appl. Climatol.* **2023**, *152*, 473–520. [[CrossRef](#)]
7. Jumin, E.; Zaini, N.; Ahmed, A.N.; Abdullah, S.; Ismail, M.; Sherif, M.; Sefelnasr, A.; El-Shafie, A. Machine learning versus linear regression modelling approach for accurate ozone concentrations prediction. *Eng. Appl. Comput. Fluid Mech.* **2020**, *14*, 713–725. [[CrossRef](#)]
8. Ehteram, M.; Ahmed, A.N.; Latif, S.D.; Huang, Y.F.; Alizamir, M.; Kisi, O.; Mert, C.; El-Shafie, A. Design of a hybrid ann multi-objective whale algorithm for suspended sediment load prediction. *Environ. Sci. Pollut. Res.* **2020**, *28*, 1596–1611. [[CrossRef](#)]
9. Sapitang, M.; Ridwan, W.M.; Faizal Kushiari, K.; Najah Ahmed, A.; El-Shafie, A. Machine learning application in reservoir water level forecasting for Sustainable Hydropower Generation Strategy. *Sustainability* **2020**, *12*, 6121. [[CrossRef](#)]
10. Tsonis, A.A.; Swanson, K.L. Topology and predictability of El Niño and La Niña Networks. *Phys. Rev. Lett.* **2008**, *100*, 228502. [[CrossRef](#)]
11. Yamasaki, K.; Gozolchiani, A.; Havlin, S. Climate networks around the globe are significantly affected by El Niño. *Phys. Rev. Lett.* **2008**, *100*, 228501. [[CrossRef](#)]
12. Stolbova, V.; Surovyatkina, E.; Bookhagen, B.; Kurths, J. Tipping elements of the Indian Monsoon: Prediction of onset and withdrawal. *Geophys. Res. Lett.* **2016**, *43*, 3982–3990. [[CrossRef](#)]
13. Nooteboom, P.D. Interactive comment on “Using network theory and machine learning to predict El Niño” by Peter D. Nooteboom et al. *Earth Syst. Dynam. Discuss.* **2018**. [[CrossRef](#)]
14. Dijkstra, H.A.; Petersik, P.; Hernández-García, E.; López, C. The application of machine learning techniques to improve El Niño prediction skill. *Front. Phys.* **2019**, *7*, 153. [[CrossRef](#)]
15. Ratnam, J.V.; Dijkstra, H.A.; Behera, S.K. A machine learning based prediction system for the Indian Ocean Dipole. *Sci. Rep.* **2020**, *10*, 284. [[CrossRef](#)] [[PubMed](#)]
16. Pal, M.; Maity, R.; Ratnam, J.V.; Nonaka, M.; Behera, S.K. Long-lead prediction of ENSO Modoki index using machine learning algorithms. *Sci. Rep.* **2020**, *10*, 365. [[CrossRef](#)] [[PubMed](#)]
17. Maity, R.; Chanda, K.; Dutta, R.; Ratnam, J.V.; Nonaka, M.; Behera, S. Contrasting features of hydroclimatic teleconnections and the predictability of seasonal rainfall over East and West Japan. *Meteorol. Appl.* **2020**, *27*, e1881. [[CrossRef](#)]
18. Cifuentes, J.; Marulanda, G.; Bello, A.; Reneses, J. Air temperature forecasting using Machine Learning Techniques: A Review. *Energies* **2020**, *13*, 4215. [[CrossRef](#)]
19. Fan, J.; Meng, J.; Ludescher, J.; Chen, X.; Ashkenazy, Y.; Kurths, J.; Havlin, S.; Schellnhuber, H.J. Statistical physics approaches to the complex Earth System. *Phys. Rep.* **2021**, *896*, 1–84. [[CrossRef](#)] [[PubMed](#)]
20. Jain, S.; Rathee, S.; Kumar, A.; Sambasivam, A.; Boadh, R.; Choudhary, T.; Kumar, P.; Kumar Singh, P. Prediction of temperature for various pressure levels using ann and multiple linear regression techniques: A case study. *Mater. Today Proc.* **2022**, *56*, 194–199. [[CrossRef](#)]
21. Hanoon, M.S.; Ahmed, A.N.; Zaini, N.; Razzaq, A.; Kumar, P.; Sherif, M.; Sefelnasr, A.; El-Shafie, A. Developing machine learning algorithms for meteorological temperature and humidity forecasting at Terengganu state in Malaysia. *Sci. Rep.* **2021**, *11*, 18935. [[CrossRef](#)]
22. Heng, S.Y.; Ridwan, W.M.; Kumar, P.; Ahmed, A.N.; Fai, C.M.; Birima, A.H.; El-Shafie, A. Artificial neural network model with different backpropagation algorithms and meteorological data for solar radiation prediction. *Sci. Rep.* **2022**, *12*, 10457. [[CrossRef](#)]
23. Sailor, D.J.; Smith, M.; Hart, M. Climate Change Implications for Wind Power Resources in the Northwest United States. *Renew. Energy* **2008**, *33*, 2393–2406. [[CrossRef](#)]

24. Pryor, S.C.; Barthelmie, R.J. Climate Change Impacts on Wind Energy: A Review. *Renew. Sustain. Energy Rev.* **2010**, *14*, 430–437. [[CrossRef](#)]
25. Cradden, L.C.; Harrison, G.P.; Chick, J.P. Will Climate Change Impact on Wind Power Development in the UK? *Clim. Change* **2012**, *115*, 837–852. [[CrossRef](#)]
26. Fant, C.; Adam Schlosser, C.; Strzepek, K. The Impact of Climate Change on Wind and Solar Resources in Southern Africa. *Appl. Energy* **2016**, *161*, 556–564. [[CrossRef](#)]
27. Taylor, K.E.; Stouffer, R.J.; Meehl, G.A. An Overview of CMIP5 and the Experiment Design. *Bull. Am. Meteorol. Soc.* **2012**, *93*, 485–498. [[CrossRef](#)]
28. Mohan, S.; Bhaskaran, P.K. Evaluation and Bias Correction of Global Climate Models in the CMIP5 over the Indian Ocean Region. *Environ. Monit. Assess.* **2019**, *191*, 806. [[CrossRef](#)] [[PubMed](#)]
29. Naveena, N.; Satyanarayana, G.C.; Rao, D.V.B.; Srinivas, D. An Accentuated “Hot Blob” over Vidarbha, India, during the Pre-Monsoon Season. *Nat. Hazards* **2020**, *105*, 1359–1373. [[CrossRef](#)]
30. Satyanarayana, G.C.; Rao, D.V.B. Phenology of Heat Waves over India. *Atmos. Res.* **2020**, *245*, 105078. [[CrossRef](#)]
31. Singh, S.; Mall, R.K.; Dadich, J.; Verma, S.; Singh, J.V.; Gupta, A. Evaluation of cordex- South Asia regional climate models for heat wave simulations over India. *Atmospheric Research* **2021**, *248*, 105228. [[CrossRef](#)]
32. Astsatryan, H.; Grigoryan, H.; Poghosyan, A.; Abrahamyan, R.; Asmaryan, S.; Muradyan, V.; Tepanosyan, G.; Guigoz, Y.; Giuliani, G. Air temperature forecasting using artificial neural network for Ararat Valley. *Earth Sci. Inform.* **2021**, *14*, 711–722. [[CrossRef](#)]
33. Copernicus Climate Change Service, Climate Data Store, (2021): In Situ Total Column Ozone and Ozone Soundings from 1924 to Present from the World Ozone and Ultraviolet Radiation Data Centre. Copernicus Climate Change Service (C3S) Climate Data Store (CDS). 2021. Available online: <https://climate.copernicus.eu/> (accessed on 11 November 2022).
34. Srivastava, A.K.; Rajeevan, M.; Kshirsagar, S.R. Development of a High Resolution Daily Gridded Temperature Data Set (1969–2005) for the Indian Region. *Atmos. Sci. Lett.* **2009**, *10*, 249–254. [[CrossRef](#)]
35. Swain, D.; Ali, M.M.; Weller, R.A. Estimation of mixed-layer depth from surface parameters. *J. Mar. Res.* **2006**, *64*, 745–758. [[CrossRef](#)]
36. Badran, F.; Thiria, S.; Crepon, M. Wind ambiguity removal by the use of neural network techniques. *J. Geophys. Res.* **1991**, *96*, 20521. [[CrossRef](#)]
37. Butler, C.T.; Meredith, R.v.Z.; Stogryn, A.P. Retrieving atmospheric temperature parameters from DMSP SSM/T-1 data with a neural network. *J. Geophys. Res. Atmos.* **1996**, *101*, 7075–7083. [[CrossRef](#)]
38. French, M.N.; Krajewski, W.F.; Cuykendall, R.R. Rainfall forecasting in space and time using a neural network. *J. Hydrol.* **1992**, *137*, 1–31. [[CrossRef](#)]
39. Ali, M.M. Estimation of ocean subsurface thermal structure from surface parameters: A neural network approach. *Geophys. Res. Lett.* **2004**, *31*, L20308. [[CrossRef](#)]
40. Jain, S.; Ali, M.M. Estimation of sound speed profiles using artificial neural networks. *IEEE Geosci. Remote Sens. Lett.* **2006**, *3*, 467–470. [[CrossRef](#)]
41. Krasnopolsky, V.M.; Breaker, L.C.; Gemmill, W.H. A neural network as a nonlinear transfer function model for retrieving surface wind speeds from the Special Sensor Microwave Imager. *J. Geophys. Res.* **1995**, *100*, 11033–11045. [[CrossRef](#)]
42. Krasnopolsky, V.M.; Schiller, H. Some neural network applications in environmental sciences. part I: Forward and inverse problems in geophysical remote measurements. *Neural Netw.* **2003**, *16*, 321–334. [[CrossRef](#)]
43. Ray, R.D.; Koblinsky, C.J.; Beckley, B.D. On the Effectiveness of Geosat Altimeter Corrections. *Int. J. Remote Sens.* **1991**, *12*, 1979–1984. [[CrossRef](#)]
44. Wilks, D.S. *Statistical Methods in the Atmospheric Sciences*; Elsevier: Amsterdam, The Netherlands, 2006.

Disclaimer/Publisher’s Note: The statements, opinions and data contained in all publications are solely those of the individual author(s) and contributor(s) and not of MDPI and/or the editor(s). MDPI and/or the editor(s) disclaim responsibility for any injury to people or property resulting from any ideas, methods, instructions or products referred to in the content.